



# An experimental and kinetic modelling study of $n$ -C<sub>4</sub>–C<sub>6</sub> aldehydes oxidation in a jet-stirred reactor

Matteo Pelucchi<sup>a,\*</sup>, Sylvain Namysl<sup>b</sup>, Eliseo Ranzi<sup>a</sup>, Alessio Frassoldati<sup>a</sup>,  
Olivier Herbinet<sup>b</sup>, Frédérique Battin-Leclerc<sup>b</sup>, Tiziano Faravelli<sup>a</sup>

<sup>a</sup> CRECK Modeling Lab, Department of Chemistry, Materials and Chemical Engineering "G. Natta", Politecnico di Milano, P.zza Leonardo da Vinci 32, 20133 Milano, Italy

<sup>b</sup> Laboratoire Réactions et Génie des Procédés, CNRS, Université de Lorraine, ENSIC, Nancy Cedex, France

Received 28 November 2017; accepted 22 July 2018

Available online 8 August 2018

## Abstract

In recent years a few experimental and kinetic modelling studies have been devoted to the understanding of the oxidation chemistry of aldehydes, because of their importance as intermediate and product species in alkane and biofuel oxidation. In this work, new jet-stirred reactor experimental data are presented for  $n$ -butanal and  $n$ -pentanal, extending the availability of targets for kinetic model validation. Consistently with previous detailed measurements on  $n$ -hexanal oxidation, experiments have been carried out for both fuels over the temperature range 475–1100 K, at a residence time of 2 s, pressure of 106.7 kPa, inlet fuel mole fraction of 0.005 and at three equivalence ratios ( $\phi = 0.5, 1$  and  $2$ ). A recently published literature model by Pelucchi et al. was used to interpret these experiments. The assumption according to which most of the C<sub>n</sub> aldehyde reactivity is controlled by the low-temperature branching pathways of the C<sub>n-1</sub> alkyl radical, allows good agreement between experiments and model in terms of fuel conversion and for most of the detected species. The systematic and comparative analysis here presented for C<sub>4</sub>–C<sub>6</sub> linear aldehydes further constrains the general rate rules, applicable to the description of higher molecular weight aldehydes, which can be produced from heavier alcohols ( $n$ -pentanol,  $n$ -hexanol etc.) and fossil fuel oxidation.

© 2018 The Author(s). Published by Elsevier Inc. on behalf of The Combustion Institute.

This is an open access article under the CC BY license. (<http://creativecommons.org/licenses/by/4.0/>)

**Keywords:** Aldehydes; Low-temperature kinetics; Jet stirred reactor; Kinetic modeling

## 1. Introduction

Pursuing a sustainable energy scenario for transportation requires the blending of renewable

oxygenated fuels (e.g. alcohols) into commercial hydrocarbon fuels. Alcohol combustion is univocally associated with an increase in the emission of toxic compounds such as aldehydes and ketones [1,2]. The synergistic development of new fuels and engine technologies [3], as well as the optimization of pyrolysis and gasification processes of biomass derived bio-oils, requires the assessment of the influence of different functional

\* Corresponding author.

E-mail address: [matteo.pelucchi@polimi.it](mailto:matteo.pelucchi@polimi.it)  
(M. Pelucchi).

groups on the reactivity of a given compound [4]. This motivates recent research efforts devoted to a better understanding of long chain aldehydes combustion [5–10]. Veloo et al. [5,6] presented laminar flame speeds and jet-stirred reactor (JSR) measurements for C<sub>3</sub>–C<sub>4</sub> aldehydes, together with a kinetic model. Pelucchi et al. [7,8] developed and validated a kinetic mechanism covering pyrolysis, high and low-temperature oxidation conditions for different aldehydes (R<sub>n</sub>-(C=O)-H) [8]. Propanal, n-butanal and n-pentanal pyrolysis and high temperature oxidation were investigated in shock tubes [7]. The kinetic model was then extended to low temperature conditions for propanal and n-butanal. The dominant H-abstraction channel at the aldehydic site forms a carbonyl radical (R<sub>n</sub>-CO), which rapidly decomposes to an alkyl radical (R<sub>n</sub>) and CO. The low-temperature oxidation of the generic C<sub>n</sub> aldehyde then falls into the low-temperature pathways typical of C<sub>n-1</sub> alkyl radicals. A further confirmation to this assumption was recently given by Serinyel et al. [10], analyzing the oxidation of two branched C<sub>5</sub> aldehydes (i.e. 2- and 3-methylbutanal) in a JSR at 500–1200 K and p = 10 atm. Indeed, *sec*-butyl and *iso*-butyl radicals were found to rule the low-temperature reactivity of 2- and 3-methylbutanal, respectively.

Recently Rodriguez et al. [9] studied the oxidation of n-hexanal in an atmospheric pressure JSR at 475–1100 K, measuring reaction products using a GC and continuous wave cavity ring-down spectroscopy (CRDS). These advanced analytical techniques allowed identifying specific low-temperature oxidation products such as cyclic ethers with a C<sub>5</sub> skeleton and multi-oxygenated C<sub>6</sub> species. The kinetic model used, despite correctly capturing the overall reactivity, was not able to explain the formation of some minor species such as acetone, propanal and acrolein.

This study aims at presenting new experimental data of n-butanal and n-pentanal oxidation, complemented by previous data on n-hexanal oxidation [9], and at refining the previous kinetic models [7–9] in order to better describe aldehydes low-temperature oxidation.

## 2. Experimental

Experiments were carried out in a heated isothermal quartz jet-stirred reactor [11,12]. Experiments were performed under steady state conditions, at 1.05 atm, at a residence time of 2 s, at temperatures ranging from 500 to 1100 K, and at three equivalent ratios of 0.5, 1 and 2 with initial fuel mole fraction of 0.005. The reactive gases, diluted in helium, entered the spherical JSR through four nozzles, positioned in the centre of the vessel, and designed in order to ensure a perfect gas mixing through turbulent jets. Thermal gradients inside the reactor were reduced by using a quartz annular

pre-heating zone prior its entrance. The residence time in this zone was negligible compared to that in the reactor. Helium and oxygen were provided by Messer (purities of 99.99% and 99.999%, respectively) with flows controlled using flow rate controllers. The liquid flow (aldehydes were provided by Sigma Aldrich, with a minimal purity of 99.5% for butanal and 97% for pentanal) was controlled using a liquid-Coriolis-flow-controller, mixed with helium and passed through an evaporator before being mixed with oxygen. The relative uncertainty in gas flow rates was assumed to be around 5%.

Using heated (at 423 K) on-line connections to avoid condensation, the gases leaving the reactors were quantified using three gas chromatographs (GCs):

- O<sub>2</sub>, CO, CO<sub>2</sub> and CH<sub>4</sub> were analyzed by a GC equipped with a thermal conductivity detector, a flame-ionization detector, and a Carbosphere packed column,
- Molecules containing up to five carbon atoms were analyzed by a GC equipped with a flame-ionization detector preceded by a methanizer and a PlotQ capillary column,
- Heavier molecules were analyzed by a GC equipped with a flame-ionization detector and a HP-5 capillary column.

Identification was made using a fourth off-line GC fitted with a Plot Q or a HP-5MS column, and coupled with a mass spectrometer. Response factors were determined by injecting calibration mixtures or using the effective carbon number method. Relative uncertainties in mole fractions were estimated to be ± 5% for species calibrated using standards (the typical uncertainty on GC measurements). For species concentrations calculated with the effective carbon number method, uncertainties are estimated to be around 10%.

## 3. Kinetic modelling

The detailed model of C<sub>3</sub>–C<sub>4</sub> aldehyde oxidation [7,8] was lumped according to procedures already discussed and adopted for many fuels [13,14]. Comparisons between the original detailed mechanism and the lumped one are reported in the Supplementary Material. The derived model, was systematically extended to describe n-pentanal and n-hexanal oxidation. Figure 1 shows the effectiveness of the lumped approach in terms of reduction of number of species. The assumption of the fast decarbonylation of carbonyl radicals [8] already allows a first reduction. Figure 1 schematically shows the lumped low-temperature oxidation mechanism of n-hexanal. Although, names of lumped isomers and samples of molecular structures are therein reported, Supplementary Material better summarizes names and molecular structures. Horizontal lumping of isomers permits to describe aldehydes

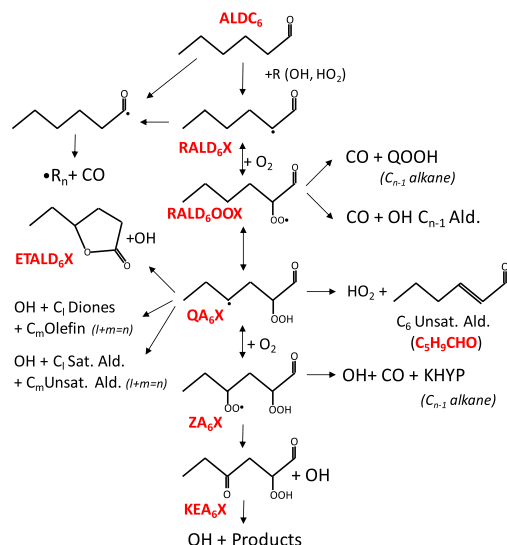


Fig. 1. Lumped kinetic mechanism of *n*-hexanal oxidation. Names and structures of some lumped C6 isomers.

mechanism with only 8 species, whereas the detailed mechanism of *n*-hexanal would need  $\sim 80$  species. This reduction within the global CRECK model is of particular interest as this model is specifically conceived to describe oxidation of real fuels, up to diesel fuels, large methyl esters ( $C_{16}$ ), biomass components [14], and also heavy PAHs ( $C_{20}$ ) precursors of soot particles.

Assuming the fast decarbonylation reaction of  $R_n$ -CO, a single radical ( $RALD_nX$ ) lumping all of the  $C_n$  aldehyde radicals carrying the unpaired electron on the alkyl moiety has been accounted for. Again, one lumped unsaturated aldehyde ( $C_nH_{2n-2}O$ ) coming from dehydrogenation reactions ( $RALD_nX = H + C_nH_{2n-2}O$ ) or from intermediate temperature pathways has been considered. At low temperatures, successive oxygen addition and isomerization reactions produce carbonyl peroxy radicals ( $RALD_nOOX$ ), alkyl carbonyl hydroperoxide radicals ( $QA_nX$ ), peroxy

carbonyl-hydroperoxide radicals ( $ZA_nX$ ) and di-carbonylhydroperoxides ( $KEA_nX$ ). Intermediate low-temperature decomposition pathways of  $QA_nX$  radicals can lead to the formation of smaller aldehydes together with smaller olefins. Moreover,  $QA_nX$  can decompose to form lactones ( $ETALD_nX$ ) and OH.

The CRECK kinetic model, obtained by extending the lumped version of  $C_3$ – $C_4$  aldehydes oxidation [7,8] to *n*-pentanal and *n*-hexanal, consists of 416 species and 11,500 reactions. In the attempt to pursue and encourage a complete unification of core mechanisms, the CRECK model was recently updated and implements a  $C_0$ – $C_3$  core mechanism obtained by coupling the  $H_2/O_2$  and  $C_1/C_2$  from Metcalfe et al. [15],  $C_3$  from Burke et al. [16], and heavier fuels from Ranzi et al. [14,17]. The thermochemical properties were adopted, when available, from [18]. The thermodynamic properties of additional fuels specific species are taken from [5,6,9]. The mechanism is provided in the Supplementary Material, together with transport and thermodynamic properties.

All simulations have been performed using the OpenSMOKE++ software [19].

#### 4. Results and discussion

Figure 2 compares experimental and predicted mole fraction profiles of the three aldehydes, at different stoichiometries. Additional comparisons are reported in the Supplementary Material (Fig. S1-S10). CRECK mechanism predicts experimental conversions quite satisfactorily. In particular, the relative reactivity both at high and low temperatures is well captured: *n*-hexanal > *n*-pentanal > *n*-butanal. In addition to the higher  $O_2$  concentration at fixed fuel content, the low-temperature reactivity is higher for heavier aldehydes also because of enhanced  $RO_2 = QOOH$  isomerization possibilities. As an example, at  $\phi = 0.5$  experimental fuel conversions at  $T = 625$  K are  $\sim 32\%$ ,  $\sim 70\%$  and  $\sim 75\%$  for *n*-butanal, *n*-pentanal and *n*-hexanal, respectively. The model slightly over-predicts *n*-butanal

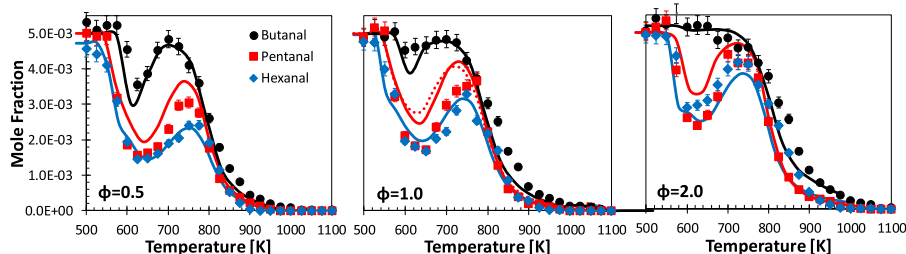


Fig. 2. Comparison of experimental (symbols) and predicted (lines) mole fraction profiles of 0.5% *n*-butanal, *n*-pentanal and *n*-hexanal [9] oxidation in an isothermal JSR,  $\phi = 0.5, 1.0, 2.0$ ,  $p = 1.05$  atm,  $\tau = 2.0$  s. Dotted line: vertical lumping, *n*-pentanal = 50%/50% (*n*-butanal/*n*-hexanal). Reported error bars: 5%.

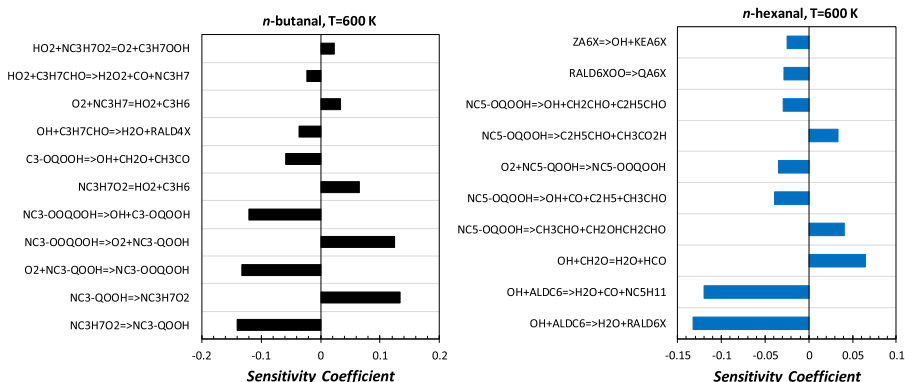


Fig. 3. Sensitivity analysis of aldehyde conversion to rate constants at  $T = 600$  K,  $\phi = 1.0$ ,  $p = 1$  atm.

conversion ( $\sim 40\%$  vs  $\sim 33\%$ ) and accurately captures *n*-hexanal low-temperature peak conversion. Conversely, the model slightly under-predicts *n*-pentanal conversion ( $\sim 61\%$  vs.  $\sim 68\%$ ). Although commercial *n*-pentanal was delivered with a declared 97% minimal purity, a GC analysis revealed a 98.8% purity. The fuel contained 0.8% of *n*-butanal and other minor impurities. Model simulations proved the negligible effect of even larger *n*-butanal impurities.

The equivalence ratio effect on the global reactivity is also correctly reproduced by the model, predicting decreasing low-temperature extents for decreasing oxygen concentrations. Aiming at a further reduction of the number of species, the dotted line in  $\phi = 1.0$  case of Fig. 2 shows pentanal fractions as obtained through the vertical lumping approach [14]. *n*-pentanal has been simply assumed as a combination of *n*-butanal (50%) and *n*-hexanal (50%). The minor discrepancies between these two predictions encourage the application of vertical lumping, when modeling heavy homologous species [20].

Results from sensitivity analyses ( $T = 600$  K,  $\phi = 1.0$ ) of aldehyde conversion to rate parameters are reported in Fig. 3 highlighting interesting features. Conditions where the low temperature reactivity of the three fuels is enough pronounced to allow for significant insights were selected. As already discussed in [8], low-temperature reactions of alkyl radicals control aldehyde low-temperature reactivity. However, H-abstraction reactions by OH and HO<sub>2</sub> radicals, from both the carbonyl and the alkyl moieties increase overall reactivity. The higher impact of H-abstractions by HO<sub>2</sub> radical for *n*-butanal is explained on the basis of a less pronounced low-temperature reactivity, as discussed above. When increasing carbon chain length, the importance of aldehyde specific low-temperature pathways increases, as it is the case for *n*-hexanal. Namely, internal isomerization (RALD6XOO = QA6X) and peroxy-carbonyl hydroperoxide radical (ZA6X) decomposition to

di-carbonyl-hydroperoxides significantly impact *n*-hexanal conversion. Most of the remaining reactions fall within propane and pentane subsets, respectively for *n*-butanal and *n*-hexanal.

To better assess model predictions, Fig. 4 shows the effects of perturbations of *n*-propylperoxy radicals isomerization rate constant ( $nC_3H_7O_2 = nC_3QOOH$ ) on *n*-butanal conversion at  $\phi = 1.0$ , for  $p = 1$  atm and 10 atm. The model over-predicts fuel conversion at atmospheric pressure, whereas under-predictions are observed at higher pressure [6]. An improved agreement could be obtained only by increasing and reducing the rate constant at high and low pressures, respectively. As expected from the limited pressure dependence of the isomerization reactions in the temperature range 550–750 K, this observation seems to indicate the presence of some inconsistencies within the two sets of

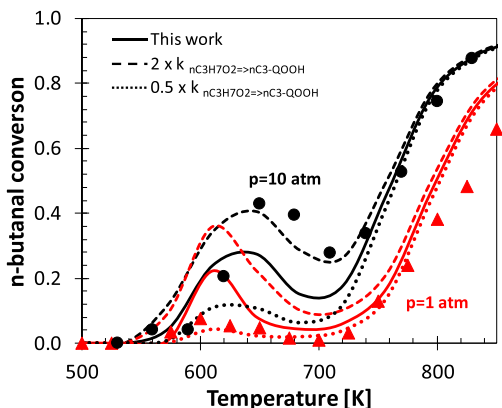


Fig. 4. Stoichiometric *n*-butanal oxidation in isothermal JSR. Experimental (symbols) [6] and predicted (lines) conversion. Red: 0.5% *n*-butanal/O<sub>2</sub>/He,  $p = 1.05$  atm,  $\tau = 2.0$  s. Black: 0.15% *n*-butanal/O<sub>2</sub>/N<sub>2</sub>,  $p = 10$  atm,  $\tau = 0.7$  s. (For interpretation of the references to color in this figure legend, the reader is referred to the web version of this article.)

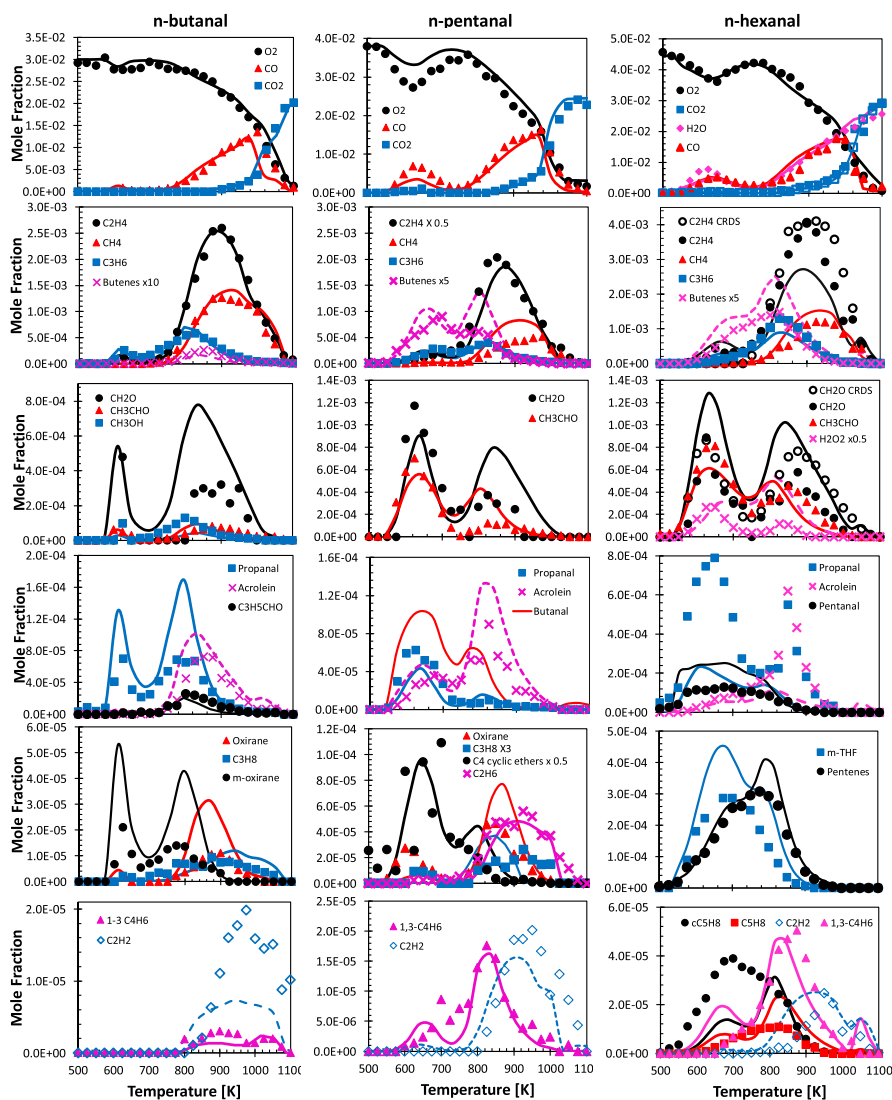


Fig. 5. *n*-butanal, *n*-pentanal and *n*-hexanal [9] oxidation in JSR at  $\phi = 1.0$ ,  $p = 1$  atm and  $\tau = 2.0$  s. Comparison between experimental (symbols) and predicted (lines) mole fraction profiles of major species.

measurements. Therefore, it is reasonable to accept a similar extent of over- and under-predictions for both datasets.

Figure 5 shows comparisons between experimental data and model predictions for selected species from the stoichiometric oxidation of the three fuels.

The model correctly predicts oxygen consumption, with largest deviations for *n*-pentanal case. Major species formation ( $\text{CO}$ ,  $\text{CO}_2$ ,  $\text{H}_2\text{O}$ ,  $\text{CH}_4$ ,  $\text{C}_2\text{H}_4$ ,  $\text{C}_3\text{H}_6$ ) is also accurately reproduced. Deviations of up to a factor of  $\sim 2$  are observed for  $\text{CH}_2\text{O}$  at  $T > 750$  K, and mainly in *n*-butanal case. In these conditions,  $\sim 80\%$  of formaldehyde comes from

the decomposition of propyl hydroperoxide radical:  $n\text{C}_3\text{-QOOH} \Rightarrow \text{OH} + \text{C}_2\text{H}_4 + \text{CH}_2\text{O}$ , whose kinetic parameters have been already assessed for propane oxidation [22]. The same reaction is responsible for  $\sim 50\%$  of formaldehyde formation at 10 atm (Figs. S3–S6). Better agreement is obtained for *n*-pentanal and *n*-hexanal. When a single model is adopted for different fuels, as it is the case for the CRECK kinetic model, *ad hoc* modifications of rate parameters according to a specific dataset strongly reduces the physical meaning of the model itself. For this reason, parameters belonging to a different kinetic subset have not been subject to modification within this study.

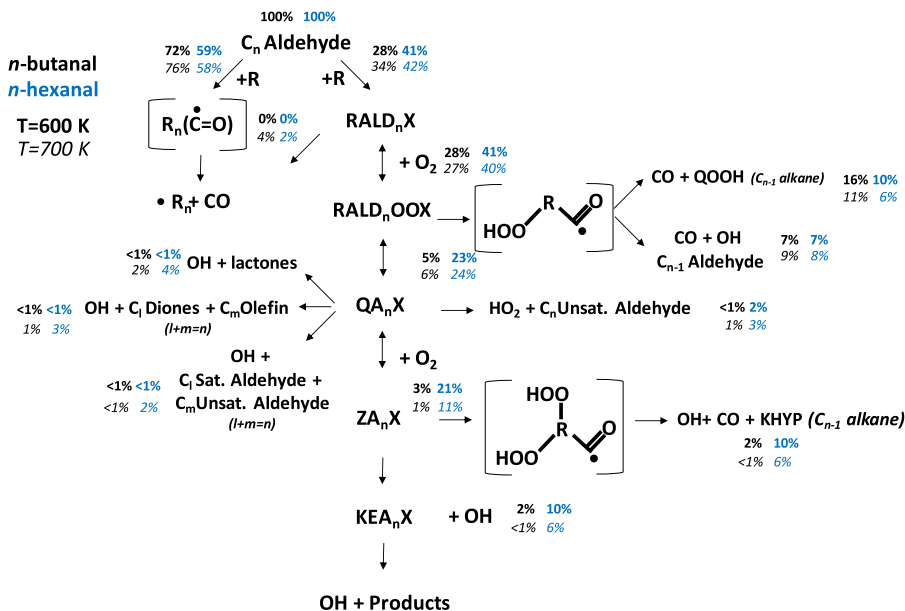


Fig. 6. Rate of production analysis of the lumped low-temperature mechanism of *n*-butanal (black) and *n*-hexanal (blue) at  $T = 600\text{ K}$  (bold) and  $T = 700\text{ K}$  (italics). Species in brackets are not explicitly accounted for in the kinetic model. Examples of specific pathways are reported in the Supplementary Material. (For interpretation of the references to color in this figure legend, the reader is referred to the web version of this article.)

Acetaldehyde formation is correctly predicted in the three cases, mainly at low temperatures where its formation is controlled by ketohydroperoxide decompositions.

At high temperatures, the same pathways control methane formation ( $CH_3 + HO_2 = O_2 + CH_4$ ) and consumption ( $CH_4 + OH = CH_3 + H_2O$ ) for the three fuels. Contributions from H-abstractions by  $CH_3$  account only for  $\sim 5$ –10%. Good agreement is found for *n*-butanal and *n*-hexanal, whereas the model over predicts methane yields in *n*-pentanal case.

Oxirane formation is also over-predicted at  $T > 800\text{ K}$ , in particular for *n*-butanal. Once again the controlling reaction is not aldehyde specific. Formation of oxirane ( $C_2H_4O1-2$ ) mostly occurs via  $C_2H_4 + HO_2 = OH + C_2H_4O1-2$ , therefore it is related to ethylene yields generally accurately predicted. Considering the uncertainties in the measurements of  $H_2O_2$  [9,21,22] the model provides relatively good predictions, mainly at low temperatures. A factor of  $\sim 10$  deviation is observed for rich cases (Fig. S10). Similar deviations were also discussed by Rodriguez et al. [9].

Cyclic ethers and olefins, mostly coming from low-temperature oxidation pathways of alkyl radicals are well captured for the three fuels. Concerning cyclic ethers, some deviations are observed for methyl-oxirane, properly predicted in propane oxidation [21].

Methanol is under-predicted by  $\sim 2.5$  times, and is controlled by H-abstractions by metoxy radical

at high temperatures. At low temperatures, contributions come from recombination disproportionation of aldehyde peroxy radicals. The importance of such reactions also for alkanes oxidation has been previously discussed [21,22]. Relatively large deviations (factor of  $\sim 2$ ) are observed for cyclopentene formation in *n*-hexanal oxidation. This species is mostly formed by the decomposition of pentylhydroperoxy radical ( $NC_5$ -QOOH) to  $HO_2$  and *n*-pentene ( $nC_5H_{10}$ ) that is further oxidized through typical low temperature pathways whose refinement is outside the scope of this study.

Figure 6 shows rate of production analysis carried out for *n*-butanal and *n*-hexanal at  $\phi = 1.0$ ,  $p = 1\text{ atm}$ ,  $T = 600$  and  $700\text{ K}$ . Flux analysis for *n*-pentanal is not reported as, from the hierarchical nature of this study, the same reaction classes explain its oxidation.

Selectivity of H-abstraction reactions on the carbonyl moiety decreases from more than 70% for *n*-butanal to less than 60% for *n*-hexanal. These percentages also reflect the relative weight of the  $C_{n-1}$  alkyl radical low-temperature oxidation. At  $T = 600\text{ K}$ , the alkyl moiety is completely oxidized by addition to  $O_2$ , while for increasing temperature a limited contribution also comes from the isomerization to directly form the carbonyl radical ( $R_{n-1} + CO$ ). Carbonyl peroxy radicals ( $RALD_nOOX$ ) isomerize to different extents to form  $QA_nX$ . At low temperature, 23% of  $RALD_nOOX$  isomerizes to  $QA_nX$  for *n*-hexanal, while only  $\sim 5\%$  successfully propagates the

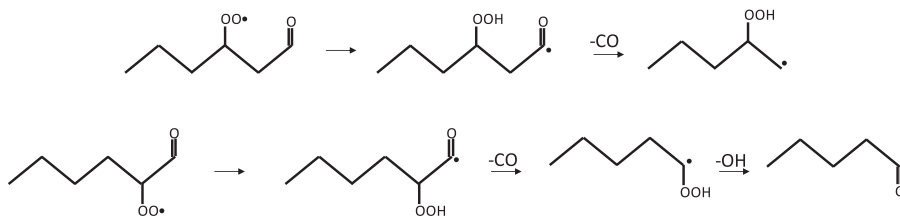


Fig. 7. Decomposition pathways of QAnX radicals with a radical position at the carbonyl moiety.

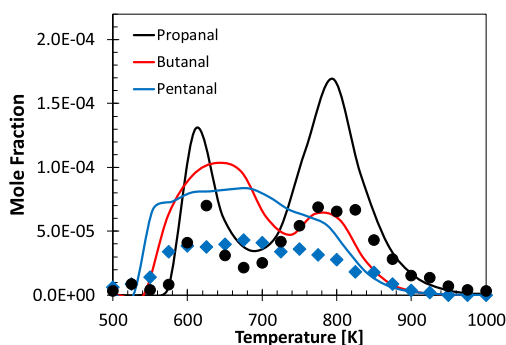


Fig. 8.  $C_{n-1}$  aldehydes formation from  $C_n$  aldehyde oxidation. Symbols: Experimental data from this study and in [9]. Lines: simulation results.

low-temperature branching in *n*-butanal case. This difference depends on molecule size and on importance of  $RALD_nOOX$  decomposition pathways.

The isomerization produces QOOH species carrying the radical at the carbonyl position, these radicals rapidly produce  $R_{n-1}$  and CO. Depending on the relative position of the  $-OOH$  group with respect to the carbonyl moiety, this step produces the QOOH radical of the  $C_{n-1}$  alkane or a  $C_{n-1}$  aldehyde and OH. The two possible channels in *n*-hexanal oxidation mechanism are depicted in Fig. 7. This pathway accounts for  $\sim 11$ – $16\%$  in butanal, and  $\sim 6$ – $11\%$  in *n*-hexanal oxidation.

Figure 8 shows the relative importance of the second channel leading to the formation of the  $C_{n-1}$

aldehyde, i.e. propanal and pentanal for *n*-butanal and *n*-hexanal, respectively. The higher concentration of  $RALD_nOOX$  in *n*-hexanal oxidation sustains the production of pentanal, whose yield does not exhibit the double maximum observed for propanal from *n*-butanal. Because of the presence of *n*-butanal as an impurity in *n*-pentanal feed (Section 3), experimental data are not reported, whereas *n*-butanal simulation profile in Fig. 8 refers to a 100% purity *n*-pentanal feed.

Decomposition channels of  $QA_nX$  are of limited impact under the conditions investigated in Fig. 6. The analogous cyclization reaction producing cyclic ethers in alkanes low-temperature oxidation, explains the formation of lactones (ETALD $_nX$ ) in the case of aldehydes. Figure 9 shows the pathways responsible for the formation of 6-methyl-tetrahydropyranone and 5-ethyl-dihydrofuranone as observed in [9]. Because of the lumped approach, the comparisons with model predictions refer to the sum of these species. The peak of lactones concentration is reproduced reasonably, despite the scarce sensitivity of model predictions to stoichiometric ratios.

A significant formation of ketones is observed for *n*-pentanal and *n*-hexanal oxidation. Figure 10 shows acetone profiles at three different equivalence ratios for *n*-hexanal. Acetone is mainly formed via the Korcek mechanism of keto-hydroperoxide decomposition, as shown in Fig. 10. This pathway was not accounted for in Rodriguez et al. [9]. The largest deviations are observed in the intermediate temperature range ( $T = 700$ – $800$  K) and mostly for the stoichiometric and the lean mixtures. The relative importance

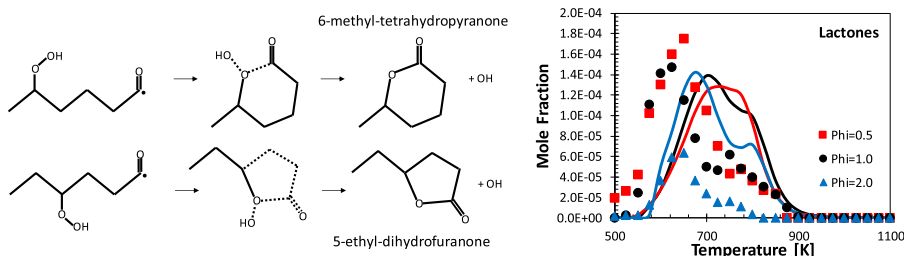


Fig. 9. *n*-hexanal oxidation. Caprolactone formation pathways and comparison between model predictions (lines) and experimental measurements (symbols) [9].

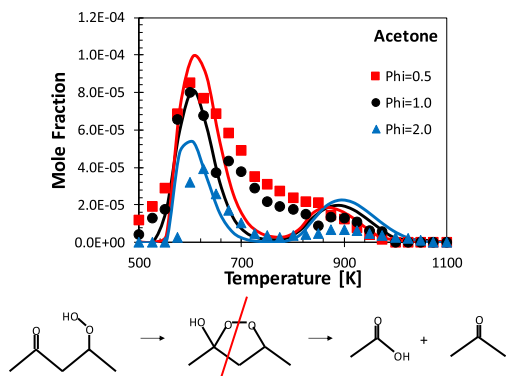


Fig. 10. *n*-hexanal oxidation. Acetone formation pathways and comparison between model (lines) and experimental measurements (symbols) [9].

of keto-hydroperoxide decomposition via O–OH bond breaking and via the Korcek mechanism already discussed by Ranzi et al. [22] (~10:1 at 750 K) directly impacts acetone yields. Clearly, a modification of this ratio toward a higher importance of the Korcek mechanism would strongly impact the low temperature branching thus worsening the agreement for fuel conversion (Fig. 2). It is worth noting that only *n*-pentanal and heavier aldehydes are expected to produce high yields of acetone as the formation of a primary alkyl radical (e.g. pent-1-yl) able to effectively isomerize to a secondary (e.g. pent-2-yl) is necessary. Moreover, a pronounced low temperature reactivity (i.e. higher ketohydroperoxide yields) favors its formation through the Korcek mechanism [22]. Finally, recombination/disproportionation reactions of peroxy radicals from  $C_{n-1}$  alkyl radicals can explain butanone formation (Fig. S11 of Supplementary Material).

## 5. Conclusions

*n*-butanal and *n*-pentanal oxidation was experimentally investigated in a JSR. Coupled with the previous measurements of *n*-hexanal oxidation [9], this study extends and completes the existing gaps in experimental targets available for the validation of aldehydes kinetic models, of relevance for the combustion of alternative fuels such as alcohols. Based on a previous study [8], and on the recent update of the core mechanism of the CRECK kinetic framework, the detailed model of aldehyde low-temperature oxidation was lumped and extended from *n*-butanal, to *n*-pentanal and *n*-hexanal, providing overall good agreement with experimental data. Aldehydes specific reaction classes were found to be responsible for some of the detected species (i.e.  $C_n$  lactones, ketones,  $C_{n-1}$  smaller aldehydes and olefins etc.). This work further constrains pathways

relevant to aldehyde oxidation, and highlights the influence of the carbonyl moiety on intermediate species formation.

### Supplementary Material “SMM”

#### SMM contains:

- Kinetic mechanism (*kinetics.CHEMKIN*, text format)
- Thermodynamics properties (*thermo.CHEMKIN*, text format)
- Supplementary\_Material.doc: additional comparisons of model and experiments, additional explanations of kinetic pathways, lumped low temperature mechanism and species nomenclature, comparison between detailed and lumped mechanism.

## Acknowledgments

The authors acknowledge the financial support of IMPROOF project (H2020-IND-CE-2016-17/H2020-SPIRE-S016) European Union’s Horizon 2020 research and innovation program (grant agreement no. 723706). Support from COST CM1404 SMARTCATs Action through the Short Term Scientific Mission is also acknowledged.

## Supplementary materials

Supplementary material associated with this article can be found, in the online version, at doi:10.1016/j.proci.2018.07.087.

## References

- [1] S.M. Sarathy, P. Oßwald, N. Hansen, K. Kohse-Höinghaus, *Prog. Energy Combust. Sci.* 44 (2014) 40–102.
- [2] E. Sadeghinezhad, S. Kazi, F. Sadeghinejad, A. Badarudin, M. Mehrali, R. Sadri, M.R. Safaei, *Renew. Sustain. Energy Rev.* 30 (2014) 29–44.
- [3] M.D. Boot, M. Tian, E.J. Hensen, S.M. Sarathy, *Prog. Energy Combust. Sci.* 60 (2017) 1–25.
- [4] M. Pelucchi, C. Cavallotti, E. Ranzi, A. Frassoldati, T. Faravelli, *Energy Fuels* 30 (2016) 8665–8679.
- [5] P.S. Veloo, P. Dagaut, C. Togbé, G. Dayma, S.M. Sarathy, C.K. Westbrook, F.N. Egolfopoulos, *Proc. Comb. Inst.* 34 (2013) 599–606.
- [6] P.S. Veloo, P. Dagaut, C. Togbé, G. Dayma, S.M. Sarathy, C.K. Westbrook, F.N. Egolfopoulos, *Combust. Flame* 160 (2013) 1609–1626.
- [7] M. Pelucchi, K.P. Somers, K. Yasunaga, U. Burke, A. Frassoldati, E. Ranzi, H.J. Curran, T. Faravelli, *Combust. Flame* 162 (2015) 265–286.
- [8] M. Pelucchi, E. Ranzi, A. Frassoldati, T. Faravelli, *Proc. Comb. Inst.* 36 (2017) 393–401.
- [9] A. Rodriguez, O. Herbinet, F. Battin-Leclerc, *Proc. Comb. Inst.* 36 (2017) 365–372.
- [10] Z. Serinyel, C. Togbé, G. Dayma, P. Dagaut, *Energy Fuels* 31 (2017) 3206–3218.
- [11] O. Herbinet, F. Battin-Leclerc, *Int. J. Chem. Kinet.* 46 (2014) 619–639.



- [12] O. Herbinet, G. Dayma, F. Battin-Leclerc, J. Simmie, E. Blurock, *Cleaner Combustion*, Springer, 2013, pp. 183–210.
- [13] E. Ranzi, M. Dente, A. Goldaniga, G. Bozzano, T. Faravelli, *Prog. Energy Combust. Sci.* 27 (2001) 99–139.
- [14] E. Ranzi, A. Frassoldati, A. Stagni, M. Pelucchi, A. Cuoci, T. Faravelli, *Int. J. Chem. Kinet.* 46 (2014) 512–542.
- [15] W.K. Metcalfe, S.M. Burke, S.S. Ahmed, H.J. Curran, *Int. J. Chem. Kinet.* 45 (2013) 638–675.
- [16] S.M. Burke, U. Burke, R. Mc Donagh, O. Mathieu, I. Osorio, C. Keesee, A. Morones, E.L. Petersen, W. Wang, T.A. DeVerter, *Combust. Flame* 162 (2015) 296–314.
- [17] E. Ranzi, A. Frassoldati, R. Grana, A. Cuoci, T. Faravelli, A. Kelley, C. Law, *Prog. Energy Combust. Sci.* 38 (2012) 468–501.
- [18] B. Ruscic, *Int. J. Quantum Chem.* 114 (2014) 1097–1101.
- [19] A. Cuoci, A. Frassoldati, T. Faravelli, E. Ranzi, *Comput. Phys. Commun.* 192 (2015) 237–264.
- [20] E. Ranzi, A. Frassoldati, S. Granata, T. Faravelli, *Ind. Eng. Chem. Res.* 44 (2005) 5170–5183.
- [21] M. Cord, B. Husson, J.C. Lizardo Huerta, O. Herbinet, P.-A. Glaude, R. Fournet, B. Sirjean, F. Battin-Leclerc, M. Ruiz-Lopez, Z. Wang, *J. Phys. Chem. A* 116 (2012) 12214–12228.
- [22] E. Ranzi, C. Cavallotti, A. Cuoci, A. Frassoldati, M. Pelucchi, T. Faravelli, *Combust. Flame* 162 (2015) 1679–1691.